

Electric-field-induced extremely large change in resistance in graphene ferromagnets

Yu Song^{1,2,*}

¹*Microsystem and Terahertz Research Center, China Academy of Engineering Physics, Chengdu 610200, P.R. China*

²*Institute of Electronic Engineering, China Academy of Engineering Physics, Mianyang 621999, P.R. China*

(Dated: July 6, 2018)

A colossal magnetoresistance ($\sim 100 \times 10^3\%$) and an extremely large magnetoresistance ($\sim 1 \times 10^6\%$) have been previously explored in manganite perovskites and Dirac materials, respectively. However, the requirement of an extremely strong magnetic field (and an extremely low temperature) makes them not applicable for realistic devices. In this work, we propose a device that can generate even larger changes in resistance in a zero-magnetic field and at a high temperature. The device is composed of a graphene under two strips of yttrium iron garnet (YIG), where two gate voltages are applied to cancel the heavy charge doping in the YIG-induced half-metallic ferromagnets. By calculations using the Landauer-Büttiker formalism, we demonstrate that, when a proper gate voltage is applied on the free ferromagnet, changes in resistance up to $305 \times 10^6\%$ ($16 \times 10^3\%$) can be achieved at the liquid helium (nitrogen) temperature and in a zero magnetic field. We attribute such a remarkable effect to a gate-induced full-polarization reversal in the free ferromagnet, which results in a metal-state to insulator-state transition in the device. We also find that, the proposed effect can be realized in devices using other magnetic insulators such as EuO and EuS. Our work should be helpful for developing a realistic switching device that is energy saving and CMOS-technology compatible.

I. INTRODUCTION

Modern hard-drive read heads and magnetoresistance random access memories are based on a tunneling magnetoresistance effect in a multilayered magnetic tunneling junction structure^{1,2}. The structure comprises one pinned and one free ferromagnets whose relative magnetization orientations can be switched between parallel and antiparallel configurations by an external magnetic field, yielding the desired low- and high-resistance states³. About two decades ago, a colossal magnetoresistance (CMR) effect with a much larger on-off ratio ($\sim 100 \times 10^3\%$)⁴, hence showing the possibility for a “next generation” computer hard drive, was found in multicomponent manganite perovskites⁵. With decreasing temperature, the materials display a transition from a paramagnetic insulator to a ferromagnetic half-metal^{6,7}. Near the transition temperature, an external magnetic field can drive the insulator to a quasi-metal⁵, yielding the “colossal” on-off ratios. A strong magnetic field is required for a relatively small low-resistance.

Several years ago, a colossal negative magnetoresistance was explored in functionalized graphene such as dilute fluorinated graphene^{8,9}. Very recently, an extremely large magnetoresistance (XMR) was explored in other Dirac materials. For example, unsaturated XMR up to $0.45 \times 10^6\%$ at 4.5 K in a magnetic field of 14.7 T and XMR up to $13 \times 10^6\%$ at 0.53 K in a magnetic field of 60 T were observed in WTe₂¹⁰, XMR of about one million percent at 2K and 9T was observed in LaSb¹¹, XMR of $0.1 \times 10^6\%$ and $0.73 \times 10^6\%$ at 2.5 K and 14 T were obtained in NbAs₂ and TaAs₂, respectively¹², and unsaturated XMR up to $11.2 \times 10^6\%$ at 1.8K in a magnetic field of 33 T was obtained in PtBi₂¹³. However, to achieve these CMR or XMR’s, extreme high-magnetic fields and low-temperatures are required. In these cases,

it is not applicable for any realistic devices yet.

In this work, we propose a device that can generate even higher on-off ratios at a high temperature and in a zero magnetic field. The device is composed of a graphene under two strips of a magnetic insulator yttrium iron garnet (YIG), where two gate voltages are applied to cancel the heavy charge doping’s in the YIG-induced half-metallic ferromagnets (see Fig. 1(a)). Based on calculations using the Landauer-Büttiker formalism, we demonstrate that, by applying a proper voltage on one of the ferromagnets (the free one), an extremely large change in resistance up to $305 \times 10^6\%$ can be achieved at the liquid helium temperature (4.2K) and in a magnetic field of 0 T. The value maintains as $16 \times 10^3\%$ at the liquid nitrogen temperature (77K). We indicate that, such huge on-off ratios stem from an electric-field-induced reversal of the full polarization in the free ferromagnet, which results in a transition between a metal and an insulator states in the device. Moreover, we find that, the proposed effect can be realized in graphene under two strips of other magnetic insulators, such as EuO and EuS.

II. DEVICE SETUP

The designed device is shown in Fig. 1(a). A sufficiently wide (in the y -direction) and short (in the x -direction) graphene strip of $L \times W$ is grown on a substrate. Here, W is several times of L to ensure that the transport is dominated by bulk states and does not depend on the edge types¹⁴. On top of the graphene, two YIG strips of lengths $l_{p,f}$ and a distance d are transferred¹⁵. As demonstrated by experiments^{15–18} and first-principle calculations¹⁹, the YIG strips induce ferromagnetism in the underlying graphene through an overlap of the spin-polarized Fe-3d states and the C- p_z

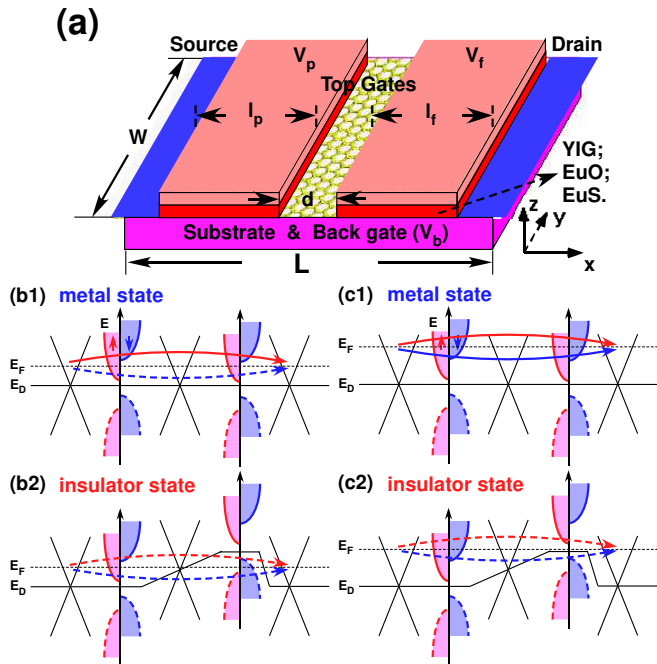


FIG. 1. Schematic diagrams for (a) the proposed device and (b,c) its metal and insulator states with half-metallic (b) or normal (c) ferromagnets. The ballistic and evanescent transports of each spin are indicated by the solid and dashed lines, respectively.

states, which is called a magnetic proximity effect. The electronic structure of the graphene ferromagnet can be described by an exchange splitting for electrons or holes (δ_e or δ_h) and a band gap opening at the Dirac point (E_G), see Fig. 2(b). Unfortunately, a heavy electron doping ($E_D = -0.78\text{eV}$) is also induced in the graphene ferromagnet^{15,19}, which limits its spintronic application by a low polarization.

On the YIG strips two top gates ($V_{p,f}$) are placed¹⁵. They are used to cancel the heavy dopings through a strong electric-field effect¹⁵ similar to that in pristine graphene²⁰. The substrate under graphene is contacting a back gate (V_b), which is used to tune the Fermi energy (E_F) through the whole device. When the Fermi energy is set as $E_F \in (E_G/2, E_G/2 + \delta_e)$ or $E_F > E_G/2 + \delta_e$, a half-metallic or normal ferromagnet of electron polarity is made use of. A small voltage (ΔV_f) is further applied on the free ferromagnet to tune its Dirac point ($E_{D,f}$). As we will see below, the Fermi energy and the Dirac point of the free ferromagnet are important to the states of the device. On the two sides of the device, the graphene film is contacted with a source and drain electrode, which may induce a contact doping (U) and a contact resistance^{21–23}. Instead of YIG, EuO and EuS can be deposited on the graphene film. The ferromagnetism is induced by an overlap of the Eu-4*f* states and the C-*p_z* states and all the parameters ($\delta_{e,h}^{(i)}$, $E_G^{(i)}$, $E_D^{(i)}$)¹⁹ as well as the Curie temperatures ($T_c^{(i)}$)^{15,24,25} become

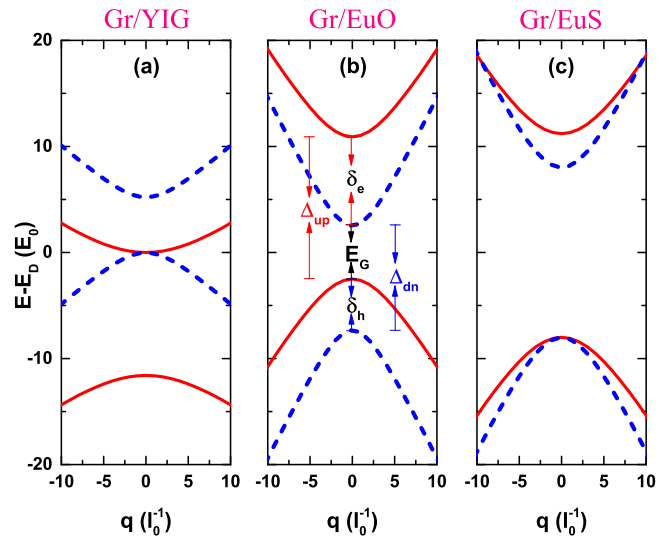


FIG. 2. Low-energy spin-resolved dispersions for graphene under (a) YIG, (b) EuO, and (c) EuS; solid for spin up and dashed for spin down. The energy ranges for the hole exchange splitting window, the Dirac gap, and the electron exchange splitting window are $(-\delta_h - E_G/2, -E_G/2)$, $(-E_G/2, E_G/2)$, and $(E_G/2, E_G/2 + |\delta_e|)$, respectively. For graphene under YIG, the energy ranges are $(-11.55E_0, -0.05E_0)$, $(-0.05E_0, 0.05E_0)$, and $(0.05E_0, 5.25E_0)$, respectively. For graphene under EuO, they read $(-7.2E_0, -2.5E_0)$, $(-2.5E_0, 2.5E_0)$, and $(2.5E_0, 10.9E_0)$, respectively. For graphene under EuS, the hole exchange splitting window disappears and the energy ranges for the other two windows are $(-8E_0, 8E_0)$ and $(8E_0, 11.2E_0)$, respectively. Here $E_0 = 10\text{meV}$ is the energy unit.

different. Here $i = 1, 2, 3$ for YIG, EuO, and EuS, respectively.

TABLE I. The Curie temperatures, Dirac cone dopings (in unit of eV), spin Dirac dopings (in unit of E_0), spin Dirac gaps (in unit of E_0), and spin Fermi velocities (in unit of v_F) for graphene under YIG, EuO, and EuS.

	T_c	$-E_D$	D_\uparrow	Δ_\uparrow	v_\uparrow	D_\downarrow	Δ_\downarrow	v_\downarrow
YIG/Gr	550K	0.78	-5.8	11.6	0.63	2.6	5.3	0.70
EuO/Gr	69K	1.37	4.2	13.4	1.337	-2.4	9.8	1.628
EuS/Gr	16.5K	1.3	1.6	18.3	1.40	0	15	1.70

III. CALCULATION FORMULA

Below we will derive the formula to calculate the device conductance at different E_F and $E_{D,f}$. Devices using YIG, EuO, and EuS will be handled uniformly.

The low-energy dispersions around the Dirac points, which are predicted by first-principle calculations^{19,26}, are re-calculated and plotted in Fig. 2. The dispersions

read

$$E_s^{(i)}(q) - E_D^{(i)} = D_s^{(i)} \pm \sqrt{(\hbar v_s^{(i)} q)^2 + (\Delta_s^{(i)}/2)^2}. \quad (1)$$

Here q is the momentum, $D_s^{(i)}$, $v_s^{(i)}$, and $\Delta_s^{(i)}$ ($s = \pm 1$ for spin up and down) are the material- and spin-dependent Dirac cone dopings, Dirac gaps, and Fermi velocities, respectively. From Fig. 2, one can see clear spin-resolved parabolic dispersions, which accompany with a band gap opening at the Dirac point and exchange splitting's for electrons and holes. The parameters for graphene on six trilayer YIG (six bilayer EuO and EuS) are given in Ref.¹⁹. The parameters in Eq. (1) relate with them by $D_{\uparrow,\downarrow}^{(i)} = \pm \delta_{e,h}^{(i)}/2$ and $\Delta_{\uparrow,\downarrow}^{(i)} = |\delta_{e,h}^{(i)}| + E_G^{(i)}$, see Fig. 2(b); $v_{\uparrow,\downarrow}$ are fitted from the original dispersions¹⁹. The values are listed in table I.

Regarding Eq. (1) as a combination of dispersions of two gapped graphene, the dispersions of the graphene ferromagnets can be described by an uniform effective Hamiltonian in a sublattice space²⁷

$$\mathcal{H}_{\mathbf{k},s,\xi}^{(i)} = \mathcal{I}(D_s^{(i)} + E_{D,f}^{(i)}) + \xi \sigma_z \Delta_s^{(i)} + \boldsymbol{\sigma} \cdot \hbar v_s^{(i)} \mathbf{k}, \quad (2)$$

where \mathcal{I} is the identity matrix, $\xi = \pm 1$ is the index for valley K and K' , $\boldsymbol{\sigma} = (\sigma_x, \sigma_y)$ is the pseudospin Pauli matrices, and $\mathbf{k} = (k, q)$ is the momentum operator. Such an effective Hamiltonian is different from those described in a sublattice-spin direct product space^{19,28,29}, where the ferromagnets are viewed as a Dirac gap and two exchange splittings. Note, in this space a four-component wave function should be solved³⁰. Different from them, in Eq. (2) we also consider a spin-resolved Fermi velocity v_s . As we will show below, this parameter would determine an effective spin Dirac gap (Δ_s/v_s) hence play an important role in the insulator state. For the graphene under the electrode metals, $\mathcal{H}_{\mathbf{k},\xi} = \mathcal{I}U + \boldsymbol{\sigma} \cdot \hbar v_F \mathbf{k}$, and for the pristine graphene between the pinned and free ferromagnets, $\mathcal{H}_{\mathbf{k},\xi} = \mathcal{I}\phi(x) + \boldsymbol{\sigma} \cdot \hbar v_F \mathbf{k}$, where $\phi(x) = (x/d)E_{D,f}$ is the potential shift.

When $E_{D,f}^{(i)} = 0$ (the cases in Fig. 1 (b1) and (c1)), the right- and left-going envelope functions in the contacted, ferromagnetic, and pristine graphene ($j = c, m, p$) can be obtained by exactly resolved $\mathcal{H}_j \Phi_j^\pm = E_j \Phi_j^\pm$. Using a characteristic energy (length) $E_0 = 10$ meV ($l_0 = \hbar v_F/E_0 = 56.55$ nm), the dimensionless result reads

$$\Phi_j^\pm = \frac{1}{\sqrt{2}E_j} \begin{pmatrix} E_j \\ \pm k_j + iq_j \end{pmatrix} e^{\pm ik_j x + iq_j y}, \quad (3)$$

where $E_{p(c)} = E(-U)$, $E_m = (E_s + \Delta_s)/v_s$ with $E_s = E - D_s(-E_{D,f})$ for the pinned (free) ferromagnet, $q_{p,c,m} = E_c \sin \alpha$ is the conserved transverse wave vector, $k_{p,c} = \text{sign}(E_{p,c})(E_{p,c}^2 - q_{p,c}^2)^{1/2}$, and $k_m = \text{sign}(E_m)(E_m E'_m - q_m^2)^{1/2}$ with $E'_m = (E_s - \Delta_s)/v_s$. It is seen that, $k_m^2 + q_m^2 = (E_s^2 - \Delta_s^2)/v_s^2$. This means that, an effective spin Dirac gap, Δ_s/v_s , is determined

by not only the spin-dependent Dirac gap but also the spin-dependent Fermi velocity.

When $E_{D,f}^{(i)} > 0$ (the cases in Fig. 1 (b2) and (c2)), the graphene between the ferromagnets becomes an n-p junction and the envelope function cannot be straightforwardly solved^{31,32}. Instead, the function can be solved in a pseudospin space which is rotated by $\pi/2$ around the y -axis (see Fig. 1(a))^{31,32}. The result reads

$$\Phi_p = c^+ \begin{pmatrix} F(x) \\ G^*(x) \end{pmatrix} e^{iq_p y} + c^- \begin{pmatrix} G(x) \\ F^*(x) \end{pmatrix} e^{iq_p y}, \quad (4)$$

where $F(x) = D[-1 + iq^2/2f, (1+i)(E+fx)/\sqrt{f}]$ and $G(x) = (1+i)\sqrt{f}q^{-1}D[iq^2/2f, (1+i)(E+fx)/\sqrt{f}]$ with $D[,]$ being the Weber parabolic cylinder function and $f = E_{D,f}/d$. Note, $F(x)$ and $G(x)$ [$F^*(x)$ and $G^*(x)$] have the properties of a right (left)-going evanescent wave function³¹. In the rotated pseudospin space, the envelope functions for the contacted and ferromagnetic graphene become $\Phi_j^\pm = [E_j \pm k_j + iq_j, -E_j \pm k_j + iq_j]^T (2E_j)^{-1} e^{\pm ik_j x + iq_j y}$.

For $T < \min(100K, T_c^{(i)})$, the ferromagnetisms hold and the inelastic scatterings (e-e and e-ph) can be ignored^{33,34}. The spin-resolved conductance through the device can be given by the Landauer-Büttiker formula³⁵

$$G_s^{(i)}(E_{D,f}, E_F, T) = G_0 \int dE \frac{-df(E, T)}{dE} \int_{-\pi/2}^{\pi/2} |t_s^{(i)}(E_{D,f}, E, \alpha)|^2 \cos \alpha d\alpha, \quad (5)$$

where $G_0 = 2e^2/h \times (|E_F|W/\hbar v_F)$ is a unit conductance, $f(E, T) = [1 + e^{(E-E_F)/k_B T}]^{-1}$ is a Fermi-Dirac distribution function, and $t_s(E_{D,f}, E, \alpha)$ is a spin-resolved transmission coefficient at a Dirac point of $E_{D,f}$, an energy of E , and an incident angle of α . $t_s^{(i)}(E_{D,f}, E, \alpha)$ can be solved by Φ_j with a standard transfer matrix method³⁶. The $E_{D,f}$ -dependent resistance of the device can be given by $R(E_{D,f}, E_F, T) = [G_\uparrow(E_{D,f}, E_F, T) + G_\downarrow(E_{D,f}, E_F, T)]^{-1}$ in unit of $R_0 = G_0^{-1}$. The changes in resistance (RC) at different $E_{D,f}$ can be defined as

$$\text{RC}^{(i)}(E_{D,f}^{(i)}, E_F, T) = \frac{R_I(E_{D,f}^{(i)}, E_F, T) - R_M(0, E_F, T)}{R_M(0, E_F, T)} \times 100\%. \quad (6)$$

To calculate a change in resistance, four conductance, $G_{\uparrow,\downarrow}(0, E_F, T)$ and $G_{\uparrow,\downarrow}(E_{D,f}, E_F, T)$, should be calculated. Each of them depends strongly on the magnetic insulator (i), ferromagnet length ($l_{p,f}$), electrode contact (U), Fermi energy (E_F), and temperature (T).

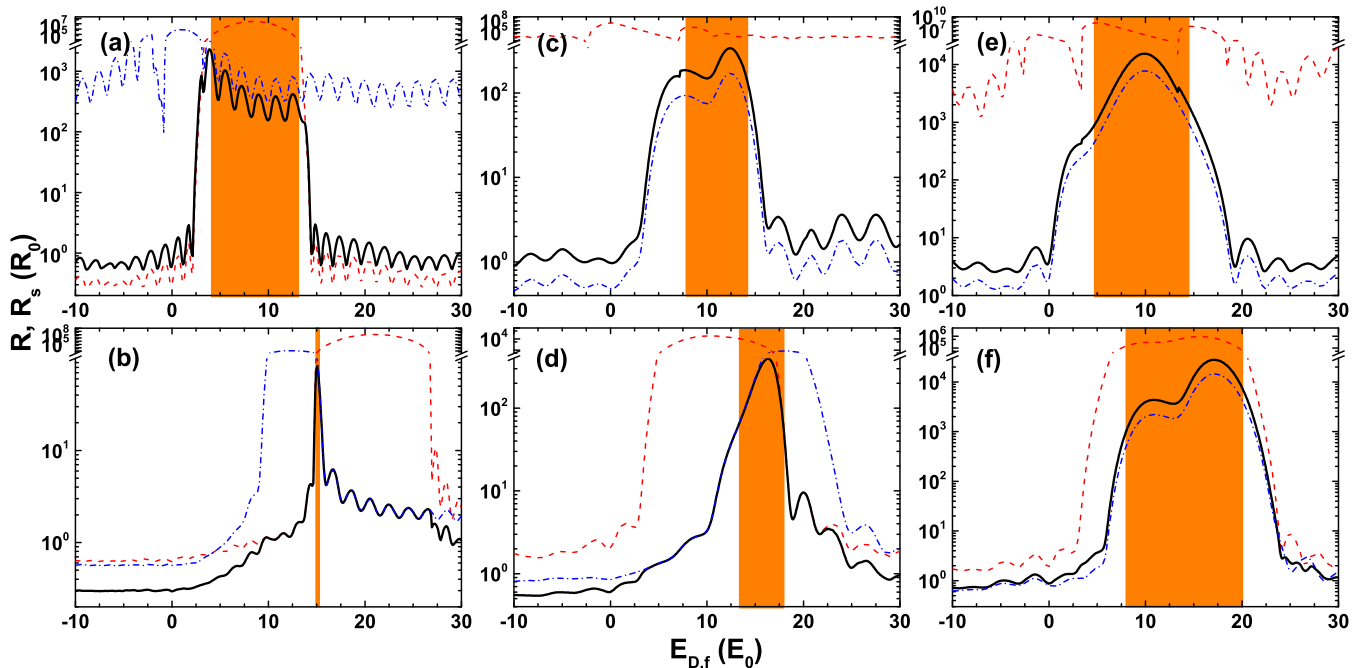


FIG. 3. The device resistance and its spin components (red dashed for spin up and blue dashed for spin down) as a function of the Dirac point shift in the free ferromagnet. The parameters are $l_p=l_f=1.0$, $d=0.5$, $U = 0$, and $E_{D,p} = 0$. (a, c, e) The cases for devices with half-metallic ferromagnets from YIG, EuO, and EuS ($E_F = 2.5, 7, 9.5$), respectively. The small (large) spin component is reduced (enlarged) by 2 times for clearness. (b, d, f) The cases for devices with normal ferromagnets from YIG, EuO, and EuS ($E_F = 15$), respectively.

IV. RESULTS AND DISCUSSION

A. Gate-induced huge changes in resistance based on metal-insulator states

We first consider a YIG-based device with two half-metallic ferromagnets ($E_F = 2.5$) of $l = 1$. Fig. 3(a) shows the zero-temperature device resistance as a function of $E_{D,f}$. As can be seen, the device resistance is rather low ($\sim 10^0 R_0$) at $E_{D,f} = 0$; it becomes rather high ($\sim 10^3 R_0$) as $E_{D,f}$ enters into the orange window. This leads to a huge on-off ratio of $3.92 \times 10^5\%$ at $E_{D,f} = 3.85$. At $E_{D,f} = 0$, both ferromagnets are half-metallic (full polarizations of spin-up). Accordingly, electrons of spin up from the device source are transparent, while electrons of spin down are blocked by two potential barriers (see Fig. 1(b1)). These behaviors result in a near-unit transmission for spin up and a rather small transmission ($\sim 10^{-6}$) for spin down, respectively, see the dashed lines in Fig. 4 (a). The transmissions respectively contribute a rather small ($0.62 R_0$) and large ($1.5 \times 10^5 R_0$) resistance, see dashed lines in Fig. 3(a). The total resistance, as a parallel connection of them, is rather small ($0.62 R_0$, almost equals to the small one). On the other hand, as can be seen in Fig. 5 (a), the low resistance increases with an increasing temperature, which implies that the device supports a metal state at $E_{D,f} = 0$.

In the orange window, $E_{D,f} \in (3.0, 13.8)$ and $E_F -$

$E_{D,f} \in (-11.3, -0.5) \in (-|\delta_h| - E_G/2, -E_G/2)$, see Fig. 2. The latter means that, the Fermi energy lies in the hole exchange splitting window of the free ferromagnet, see Fig. 1(b2). Importantly, the reversal of the charge polarity leads to an reversal of the spin polarization. In other words, by a proper $E_{D,f}$ the spin-up full polarization in the free ferromagnet becomes a spin-down full polarization. As a result, electrons of spin up from the device source, which are transparent before, now encounter a barrier in the free ferromagnet. On the other hand, electrons of spin down from the device source, which are blocked by two barriers before, now are still blocked by a barrier in the pinned ferromagnet (see Fig. 1(b2)). These behaviors are clearly reflected by the extremely suppressed transmissions ($\sim 10^{-5}$) and rather high resistances ($4.8 \times 10^4 R_0$ and $2.4 \times 10^3 R_0$) for both spins, as shown in Fig. 4 (a) and Fig. 3(a). The total resistance, as a parallel connection of two huge spin resistances, becomes rather high ($2.3 \times 10^3 R_0$). Besides the electric-field induced full-polarization reversal, the electric-field induced n-p junction also contributes to the high resistance state. This is because the transmissions become selective^{37,38}. In Fig. 5 (a), we find that the high resistance decreases with an increasing temperature, which implies that the device now supports an insulator state.

The resistances of the same device but with normal ferromagnets ($E_F = 15$) are plotted in Fig. 3 (b) as a function of $E_{D,f}$. Similar metal state at zero volt-

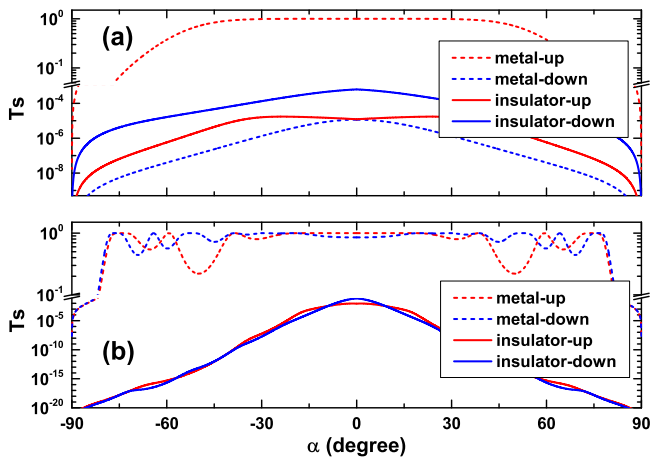


FIG. 4. (a) The spin-dependent transmissions for the metal (dashed) and insulator (solid) states based on half-metallic ferromagnets. Red for spin up and blue for spin down. (b) The spin-dependent transmissions for the metal (dashed) and insulator (solid) states based on normal ferromagnets.

age and insulator state at a proper voltage are found. The resulting on-off ratio reads $1.7 \times 10^4\%$. However, it is noticed that, the $E_{D,f}$ range for the insulator state is different from that in Fig. 3(a) and it becomes much narrower. In the orange window, it is found that $E_F - E_{D,f} \in (-E_G/2, +E_G/2)$ ($E_{D,f} \approx 15.05$), which means that, the Fermi energy enters into the Dirac gap of the free ferromagnet. As a result, electrons of both spins from the device source encounter potential barriers in the free ferromagnet, see Fig. 1(c2). This is clearly reflected by the rather small transmissions ($< 10^{-4}$) and the rather high resistances ($381R_0$ and $105R_0$) for both spins, see Fig. 4(b) and Fig. 3(b), respectively. The case is rather different from the zero voltage case, for which both spins transport over barriers (see Fig. 1(c1)) and result in near-unit transmissions in Fig. 4(b) and small resistances ($0.62R_0$ and $0.57R_0$) in Fig. 3(b).

From the above results and discussions we can see that, colossal changes in resistance, which require a strong magnetic field in manganite perovskites, can be realized by a small gate voltage in the proposed device. The underlying mechanism is that, the gate induces either a full-polarization reversal in a half-metallic ferromagnet or an energy gap in a normal ferromagnet, which results in a metal-insulator state of the device. For the former case, the insulator state arises because different spins are blocked in different ferromagnets, while for the latter case, both spins are blocked in the free ferromagnet. The energy gap (1meV) is rather narrow and will be measured out at high temperature. In following we will focus on metal-insulator states stemming from the full-polarization reversal.

Can the remarkable effect be realized in other systems? In Fig. 3(c-f) we plot the calculation results for devices with ferromagnets induced by EuO and EuS. The half-metallic ferromagnet cases based on EuO ($E_F = 7$) and

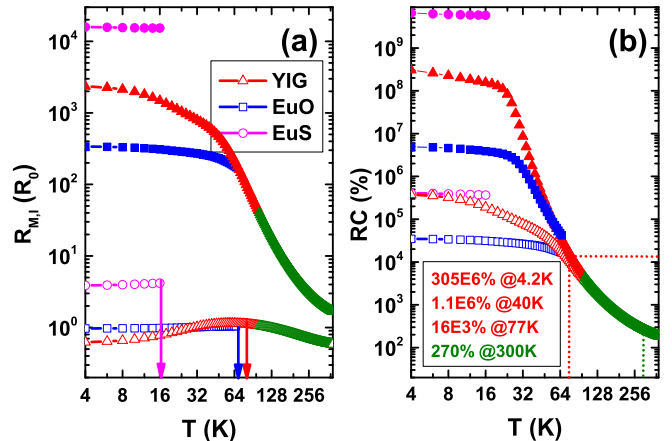


FIG. 5. (a) The resistances of metal (solid) and insulator (hollow) states for devices of $l = 1$ based on YIG (red), EuO (blue), and EuS (magenta) as a function of temperature. (b) The change in resistance for devices of $l = 2$ (solid) and $l = 1$ (dashed) based on YIG (red), EuO (blue), and EuS (magenta) as a function of temperature.

EuS ($E_F = 9.5$) are shown in Fig. 3(c) and (e), and the normal ferromagnet cases based on them ($E_F = 15$) are shown in Fig. 3(d) and (f), respectively. It is seen that, the device resistance shows similar dependence on the Dirac point of the free ferromagnet as the YIG cases. The resulting CMR are $3.5 \times 10^4\%$, $6.53 \times 10^4\%$, $4.1 \times 10^5\%$, and $3.18 \times 10^6\%$ for Figs. 3(c-f), respectively. Meanwhile, the low and high resistance at zero and proper $E_{D,f}$ show similar temperature dependence as the YIG cases (see Fig. 5(a)). The above behaviors mean that the voltage-induced metal-insulator states and huge changes in resistance can also be realized in devices based on other magnetic insulators.

B. Ferromagnet-length dependence of the on-off ratios

In all the above calculations, the ferromagnet length is fixed as l_0 ; what will happen when it is changed? In Fig. 6(a) we plot the on-off ratio of the YIG-based device as a function of the lengths of the pinned and free ferromagnets. Surprisingly, it is found that, the on-off ratio is rather sensitive to the lengths; it shows a near-exponential dependence on the ferromagnet lengths excepting $1 < l_{p,f} < 1.5$. When the ferromagnet lengths increase from 1 to 2, an extremely large on-off ratio up to $3.72 \times 10^8\%$ arises.

The strong enhancement can be understood as following. The insulator state of the device stems from evanescent transports of both spins, for which the longitudinal wave $e^{ik_m x}$ in Eq.(3) becomes an evanescent wave $e^{-\kappa x}$, where $\kappa^2 = -k_m^2$. As a result, the transmission and conductance decreases near-exponentially with an increasing barrier length. Hence, the resistance increases near-

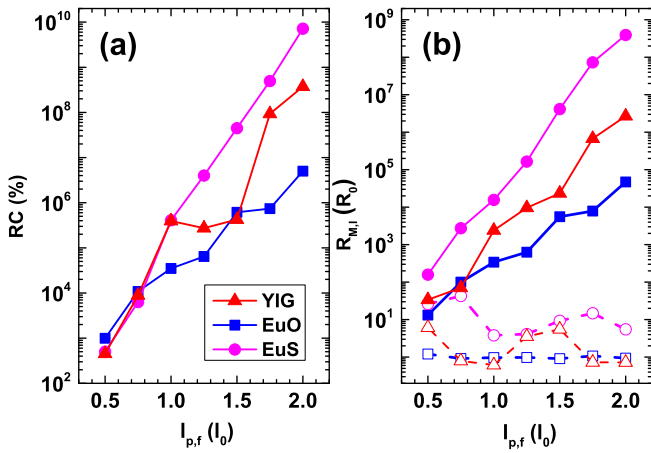


FIG. 6. (a) The change in resistance as a function of the ferromagnet lengths for devices based on YIG (red), EuO (blue), and EuS (magenta). (b) The corresponding on-state (dashed) and off-state (solid) resistances.

exponentially with an increasing length, see the red solid line in Fig. 6(b). In contrast, the metal state stems from a ballistic transport of spin up, for which $e^{ik_m x}$ is a plane wave. Accordingly, the transmission, conductance, and resistance show a weak oscillating dependence on the ferromagnet length, see the red dashed line in Fig. 6(b). The enhancement of the on-off ratio follows that of the insulator state.

The cases for devices using EuO and EuS are also plotted in Fig. 6. It is seen that, both the metal-insulator states and the on-off ratio show similar length dependence as the device using YIG. However, the slopes of the profiles are different. For the device using YIG, the change in resistance increases from $3.92 \times 10^5\%$ at $l_{p,f} = 1$ to $3.72 \times 10^8\%$ at $l_{p,f} = 2$; for the device using EuO, the on-off ratio changes from $3.50 \times 10^4\%$ to $5.00 \times 10^6\%$, while for the device using EuS, the values read $4.08 \times 10^5\%$ and $7.14 \times 10^9\%$. An enhancement factor, $\Delta(\log RC)/\Delta l_{f(p)}$, can be calculated as ~ 3 , 2 , and 4 , respectively. Interestingly, they are found to be proportional to the squares of the smaller effective spin Dirac gaps (but not the smaller spin Dirac gap itself), i.e., $\Delta RC^{(i)} \propto e^{-(\Delta_{\downarrow}^{(i)}/v_{\downarrow}^{(i)})^2 \Delta l}$. This is because the resistance is dominated by the spin with a smaller κ (i.e., spin down for all the three magnetic insulators, see table I), and $\kappa^2 \propto -\Delta_{\downarrow}^2/v_{\downarrow}^2$ near the spin Dirac points.

C. Temperature dependence of the changes in resistance

Till now, we only consider the zero-temperature on-off ratios. How it will change at high temperatures, especially at the liquid helium and the liquid nitrogen temperatures? In Fig. 5(b), we plot the numerical results for $l = 2$ (the red solid line) as a function of tempera-

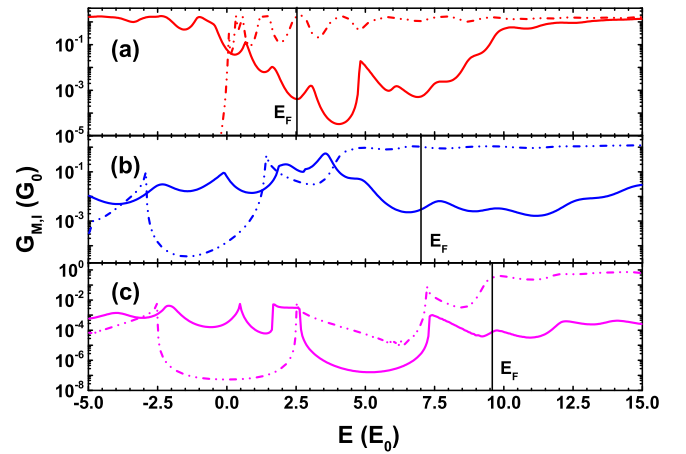


FIG. 7. The zero-temperature G_M (dashed) and G_I (solid) as a function of energy for devices of $l = 1$ based on YIG (a), EuO (b), and EuS (c).

ture. As can be seen, the on-off ratio shows a decreasing dependence on the temperature, which is similar to the temperature dependence found in manganite perovskites and other Dirac materials. However, the on-off ratio maintains $305 \times 10^6\%$ (18% smaller than the value at zero temperature) at the liquid helium temperature. This value is hundreds of times higher than the XMR previously reported in other Dirac materials at several K and under magnetic fields of several T^{10–13}. The change in resistance maintains as $16 \times 10^3\%$ at the liquid nitrogen temperature, which is still comparable with the CMR observed in manganite perovskites at the same temperature and under magnetic fields of several T⁴. The Curie temperature of the YIG-induced graphene ferromagnet is higher than the room temperature. We have also calculated the on-off ratio at the room temperature by ignoring the inelastic scattering. A change in resistance of 270% is found. The temperature dependence for a device of $l = 1$ is also shown, see the red dashed line in Fig. 5(b). It is found that, the on-off ratios are much smaller and the temperature dependence is much gentler. Moreover, the higher the temperature, the smaller the difference of the on-off ratios for different ferromagnet lengths. It is noted that, the magnetic-field-induced CMR in manganite perovskites exists only near the zero-field transition temperature; the above results show that the proposed electric-field-induced extremely large on-off ratios can survive for a wide range of high temperature.

The decreasing temperature behavior of the on-off ratio stems from the increase behavior of the low-resistance state and the decrease behavior of the high-resistance state, which are also important evidences for a metal or insulator behavior. In following we will show that these behaviors stem from a negative and positive energy dependence of the zero-temperature conductance around the Fermi energy, respectively, see Fig. 7. Due to Eq. (5), a spin-dependent current at a finite temperature T is determined by the zero-temperature currents in an es-

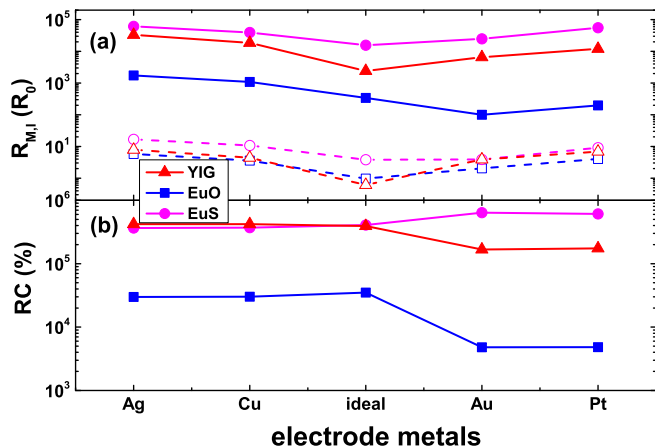


FIG. 8. (a) The on-state and off-state resistances and (b) the change in resistance for devices based on YIG (red), EuO (blue), and EuS (magenta) for several contact doping.

timated energy range $\sim (E_F - 5T, E_F + 5T)$. In Fig. 7 we plot the zero-temperature metal-insulator conductances ($G_{M,I}$) as a function of energy around the Fermi energy. As can be seen, $G_{M(I)}$ reaches almost the maximum (minimum) around the Fermi energy, which are direct results of the electronic structure as shown in Fig. 2. Accordingly, the higher the temperature, i.e., the wider the energy range, the smaller (bigger) the finite-temperature $G_{M(I)}$ and $R_{I(M)}$. An abnormal decreasing of R_M above $T > 58\text{K}$ is also observed. It stems from a “W”-shaped G_M-E profile.

The devices using EuO and EuS show similar temperature dependence (Fig. 5(b)) and underlying mechanisms (Fig. 7). However, the temperature ranges are much smaller. At the liquid helium temperature, extremely large changes in resistance up to $4.9 \times 10^6\%$ and $6.5 \times 10^9\%$ are obtained, respectively.

D. Metal contacting effects

At last, we consider the influence of metal contacts on the changes in resistance. Several familiar metals, Ag, Cu, Au, and Pt at their equilibrium distances with graphene are considered. The contact doping’s (U/E_0) equal -32, -17, 19, and 32, respectively³⁹. The calculated results are shown in Fig. 8. It is observed that, for device using YIG and EuS, both R_I and R_M increase as the contacts become non-ideal; the heavier the contact doping, the larger the resistances increase. This is because the contacting resistances are in series with the original ones. However, the low and high resistances increase differently. As a result, the on-off ratio can show different behaviors. It decreases for device using YIG (EuS) with positive (negative) doping’s, while increases

for device using YIG (EuS) with negative (positive) doping’s. Considering that the contact resistance is usually harmful for device performance⁴⁰, the latter is a rather interesting and useful result. For device using EuO, the change in resistance always decreases, slightly for negative contact doping’s and sharply for positive contact doping’s.

V. CONCLUSION

In summary, we have proposed a device that can generate extremely large changes in resistance at high temperatures and in a zero magnetic field. The device is composed of a graphene under two YIG strips, where gate voltages are applied. Based on conductance calculations we have demonstrated that, by applying a proper gate on the free ferromagnet, an on-off ratio up to $305 \times 10^6\%$ can be obtained at the liquid helium temperature and in a zero magnetic field. This value is hundreds of times higher than the XMR previously observed in Dirac materials at similar temperatures and under magnetic fields of several T. The change in resistance maintains as $16 \times 10^3\%$ at the liquid nitrogen temperature and in a zero magnetic field, which is still comparable with the CMR observed in manganite perovskites at the same temperature and under magnetic fields of several T. We have indicated that, the underlying mechanism for such a remarkable effect is that, an electric field induces a reversal of the full polarization in the half-metallic free ferromagnet, which results in metal-insulator states in the device.

Interesting results also contain: 1) the change in resistance shows a near-exponential dependence on the ferromagnet lengths, 2) the longer the two ferromagnets, the sharper the negative temperature-dependence of the on-off ratio, and 3) the effective spin Dirac gap instead of the spin Dirac gap itself plays an important role in the insulator state. We have also shown that, the proposed effect can be realized in devices using other magnetic insulators such as EuO and EuS. Our work should be helpful for developing a realistic switching device. Using an electric field instead of a magnetic field, the proposed device is also far more energy saving and compatible with the ubiquitous voltage-controlled semiconductor technology^{41–43}.

ACKNOWLEDGEMENTS

I’d like to thank M.S. XL Feng and Dr. SY Hou for inspiring discussions. This work was supported by the National Natural Science Foundation of China (Grant No. 11404300) and the Science Challenge Project (Grant No. TZ2016003-1).

- * Corresponding author; kwungyusung@gmail.com
- ¹ S. Wolf, D. Awschalom, R. Buhrman, J. Daughton, S. Von Molnar, M. Roukes, A. Y. Chtchelkanova, and D. Treger, *Science* **294**, 1488 (2001).
 - ² I. Žutić, J. Fabian, and S. D. Sarma, *Rev. Mod. Phys.* **76**, 323 (2004).
 - ³ C. Chappert, A. Fert, and F. N. Van Dau, *Nature Mater.* **6**, 813 (2007).
 - ⁴ S. Jin, T. Tiefel, M. McCormack, R. Fastnacht, R. Ramesh, and L. Chen, *Science* **264**, 413 (1994).
 - ⁵ A. Ramirez, *J. Phys. Condens. Matter.* **9**, 8171 (1997).
 - ⁶ S. Satpathy, Z. S. Popović, and F. R. Vukajlović, *Phys. Rev. Lett.* **76**, 960 (1996).
 - ⁷ J.-H. Park, E. Vescovo, H.-J. Kim, C. Kwon, R. Ramesh, and T. Venkatesan, *Nature* **392**, 794 (1998).
 - ⁸ X. Hong, S.-H. Cheng, C. Herding, and J. Zhu, *PHYSICAL REVIEW B* **83**, 085410 (2011).
 - ⁹ V. Georgakilas, M. Otyepka, A. B. Bourlinos, V. Chandra, N. Kim, K. C. Kemp, P. Hobza, R. Zboril, and K. S. Kim, *Chemical Reviews* **112**, 6156 (2012).
 - ¹⁰ M. Ali, J. Xiong, S. Flynn, J. Tao, Q. Gibson, L. Schoop, T. Liang, N. Haldolaarachchige, M. Hirschberger, N. Ong, and R. Cava, *Nature* **514**, 205 (2014).
 - ¹¹ F. Tafti, Q. Gibson, S. Kushwaha, N. Haldolaarachchige, and R. Cava, *Nature Phys.* **12**, 272 (2015).
 - ¹² Y.-Y. Wang, Q.-H. Yu, P.-J. Guo, K. Liu, and T.-L. Xia, *Phys. Rev. B* **94**, 041103 (2016).
 - ¹³ W. Gao, N. Hao, F.-W. Zheng, W. Ning, M. Wu, X. Zhu, G. Zheng, J. Zhang, J. Lu, H. Zhang, *et al.*, *Phys. Rev. Lett.* **118**, 256601 (2017).
 - ¹⁴ J. Tworzydło, B. Trauzettel, M. Titov, A. Rycerz, and C. W. J. Beenakker, *Phys. Rev. Lett.* **96**, 246802 (2006).
 - ¹⁵ Z. Wang, C. Tang, R. Sachs, Y. Barlas, and J. Shi, *Phys. Rev. Lett.* **114**, 016603 (2015).
 - ¹⁶ J. Mendes, O. A. Santos, L. Meireles, R. Lacerda, L. Vilela-Leão, F. Machado, R. Rodríguez-Suárez, A. Azevedo, and S. Rezende, *Phys. Rev. Lett.* **115**, 226601 (2015).
 - ¹⁷ J. C. Leutenantsmeyer, A. A. Kaverzin, M. Wojtaszek, and B. J. van Wees, *2D Mater.* **4**, 014001 (2016).
 - ¹⁸ M. Evelt, H. Ochoa, O. Dzyapko, V. E. Demidov, A. Yurgens, J. Sun, Y. Tserkovnyak, V. Bessonov, A. B. Rinkevich, and S. O. Demokritov, *Phys. Rev. B* **95**, 024408 (2017).
 - ¹⁹ A. Hallal, F. Ibrahim, H. Yang, S. Roche, and M. Chshiev, *2D Mater.* **4**, 025074 (2017).
 - ²⁰ K. S. Novoselov, A. K. Geim, S. V. Morozov, D. Jiang, Y. Zhang, S. V. Dubonos, I. V. Grigorieva, and A. A. Firsov, *Science* **306**, 666 (2004).
 - ²¹ F. Xia, V. Perebeinos, Y.-m. Lin, Y. Wu, and P. Avouris, *Nature Nanotech.* **6**, 179 (2011).
 - ²² J. A. Robinson, M. LaBella, M. Zhu, M. Hollander, R. Kasarda, Z. Hughes, K. Trumbull, R. Cavallero, and D. Snyder, *Appl. Phys. Lett.* **98**, 053103 (2011).
 - ²³ S. M. Song, J. K. Park, O. J. Sul, and B. J. Cho, *Nano Lett.* **12**, 3887 (2012).
 - ²⁴ A. G. Swartz, P. M. Odenthal, Y. Hao, R. S. Ruoff, and R. K. Kawakami, *ACS Nano* **6**, 10063 (2012).
 - ²⁵ P. Wei, S. Lee, F. Lemaitre, L. Pinel, D. Cutaia, W. Cha, F. Katmis, Y. Zhu, D. Heiman, J. Hone, *et al.*, *Nature Mater.* **15**, 711 (2016).
 - ²⁶ H.-X. Yang, A. Hallal, D. Terrade, X. Waintal, S. Roche, and M. Chshiev, *Phys. Rev. Lett.* **110**, 046603 (2013).
 - ²⁷ C. Beenakker, *Rev. Mod. Phys.* **80**, 1337 (2008).
 - ²⁸ K. Zollner, M. Gmitra, T. Frank, and J. Fabian, *Phys. Rev. B* **94**, 155441 (2016).
 - ²⁹ S. Su, Y. Barlas, J. Li, J. Shi, and R. K. Lake, *Phys. Rev. B* **95**, 075418 (2017).
 - ³⁰ Y. Song and H.-C. Wu, *J. Phys. Condens. Matter.* **25**, 355301 (2013).
 - ³¹ E. Sonin, *Phys. Rev. B* **79**, 195438 (2009).
 - ³² Y. Song, H.-C. Wu, and Y. Guo, *Appl. Phys. Lett.* **102**, 093118 (2013).
 - ³³ S. Morozov, K. Novoselov, M. Katsnelson, F. Schedin, D. Elias, J. A. Jaszczak, and A. Geim, *Phys. Rev. Lett.* **100**, 016602 (2008).
 - ³⁴ J.-H. Chen, C. Jang, S. Xiao, M. Ishigami, and M. S. Fuhrer, *Nature Nanotech.* **3**, 206 (2008).
 - ³⁵ M. Büttiker, Y. Imry, R. Landauer, and S. Pinhas, *Phys. Rev. B* **31**, 6207 (1985).
 - ³⁶ M. Born and E. Wolf, *Principles of optics: electromagnetic theory of propagation, interference and diffraction of light* (Elsevier, 1980).
 - ³⁷ V. V. Cheianov and V. I. Falko, *Phys. Rev. B* **74**, 041403 (2006).
 - ³⁸ V. V. Cheianov, V. Fal'ko, and B. Altshuler, *Science* **315**, 1252 (2007).
 - ³⁹ G. Giovannetti, P. Khomyakov, G. Brocks, V. v. Karpan, J. Van den Brink, and P. Kelly, *Phys. Rev. Lett.* **101**, 026803 (2008).
 - ⁴⁰ S. Russo, M. Craciun, M. Yamamoto, A. Morpurgo, and S. Tarucha, *Phys. E* **42**, 677 (2010).
 - ⁴¹ D. Chiba, M. Sawicki, Y. Nishitani, Y. Nakatani, F. Matsukura, and H. Ohno, *Nature* **455**, 515 (2008).
 - ⁴² H. Ohno, *Nature Mater.* **9**, 952 (2010).
 - ⁴³ F. Matsukura, Y. Tokura, and H. Ohno, *Nature Nanotech.* **10**, 209 (2015).